

1 **Early warnings and missed alarms for abrupt monsoon transitions**

2

3 **Authors:** Zoë A. Thomas^{1,2*}, Frank Kwasniok³, Chris A. Boulton², Peter M. Cox³, Richard
4 T. Jones², Timothy M. Lenton², Chris S.M. Turney¹

5

6 **Affiliations**

7 ¹Climate Change Research Centre and School of Biological, Earth & Environmental
8 Sciences, University of New South Wales, Sydney, NSW 2052, Australia

9 ²College of Life and Environmental Science, University of Exeter, Exeter, EX4 4RJ, UK

10 ³College of Engineering, Mathematics and Physical Sciences, University of Exeter, Exeter,
11 EX4 4QF, UK

12 * E-mail: z.thomas@unsw.edu.au

13

14 **Abstract**

15 Palaeo-records from China demonstrate that the East Asian Summer Monsoon (EASM) is
16 dominated by abrupt and large magnitude monsoon shifts on millennial timescales,
17 switching between periods of high and weak monsoon rains. It has been hypothesised that
18 over these timescales, the EASM exhibits two stable states with bifurcation-type tipping
19 points between them. Here we test this hypothesis by looking for early warning signals of
20 past bifurcations in speleothem $\delta^{18}\text{O}$ records from Sanbao Cave and Hulu Cave, China,
21 spanning the penultimate glacial cycle. We find that although there are increases in both
22 autocorrelation and variance preceding some of the monsoon transitions during this period,
23 it is only immediately prior to the abrupt monsoon shift at the penultimate deglaciation
24 (Termination II) that statistically significant increases are detected. To supplement our data
25 analysis, we produce and analyse multiple model simulations that we derive from these

26 data. We find hysteresis behaviour in our model simulations with transitions directly forced
27 by solar insolation. However, signals of critical slowing down, which occur on the approach
28 to a bifurcation, are only detectable in the model simulations when the change in system
29 stability is sufficiently slow to be detected by the sampling resolution of the dataset. This
30 raises the possibility that the early warning ‘alarms’ were missed in the speleothem data
31 over the period 224-150 ka BP and it was only at the monsoon termination that the change
32 in the system stability was sufficiently slow to detect early warning signals.

33

34 **Keywords: Speleothem, monsoon, bifurcation, early warning signals, tipping point**

35

36 **1. Introduction**

37 The Asian Summer Monsoon directly influences over 60% of the world’s population (Wu et
38 al., 2012) and yet the drivers of past and future variability remain highly uncertain
39 (Levermann et al., 2009; Zickfeld et al., 2005). Evidence based on radiometrically-dated
40 speleothem records of past monsoon behaviour from East Asia (Yuan et al., 2004) suggests
41 that on millennial timescales, the EASM is driven by a 23 kyr precession cycle (Kutzbach,
42 1981; Wang et al., 2008), but also influenced by feedbacks in sea surface temperatures and
43 changing boundary conditions including Northern Hemisphere ice volume (An, 2000; Sun
44 et al., 2015). The demise of Chinese dynasties have been linked to monsoon shifts over
45 more recent millennia (Zhang et al., 2008), suggesting that any future changes, whether
46 caused by solar or anthropogenic forcing, could have similarly devastating societal impacts.
47 The abrupt nature of the monsoon behaviour in comparison to the sinusoidal insolation
48 forcing strongly implies that this response is non-linear (Figure 1); whilst Northern
49 Hemisphere Summer Insolation (NHSI) follows a quasi-sinusoidal cycle, the $\delta^{18}\text{O}$ profile in

50 speleothems exhibits a step function, suggesting the presence of threshold behaviour in the
51 monsoon system (Schewe et al., 2012).

52

53

54 **Figure 1:** (a) Northern Hemisphere Summer Insolation (NHSI) at June 30°N (Berger and
55 Loutre, 1991) (grey), $\delta^{18}\text{O}$ speleothem data from Sanbao Cave (Wang et al., 2008) (dark
56 blue), (b) $\delta^{18}\text{O}$ speleothem data from Hulu Cave (Wang et al., 2001); speleothem MSH
57 (red), MSP (blue) and MSX (yellow), (c) CO_2 (ppmv) from the Antarctic Vostok ice core
58 (Petit et al., 1999) (black), (d) $\delta^{18}\text{O}$ per mille benthic carbonate (Lisiecki and Raymo, 2005)
59 (proxy for global ice volume) (purple).

60

61

62 A minimum conceptual model of the East Asian Summer Monsoon developed by Zickfeld
63 et al. (2005), stripped down by Levermann et al. (2009) and updated by Schewe et al.
64 (2012), shows a non-linear solution structure with thresholds for switching a monsoon
65 system between ‘on’ or ‘off’ states that can be defined in terms of atmospheric humidity –
66 in particular, atmospheric specific humidity over the adjacent ocean (Schewe et al., 2012).
67 Critically, if specific humidity levels pass below a certain threshold, for instance, as a result
68 of reduced sea surface temperatures, insufficient latent heat is produced in the atmospheric
69 column and the monsoon fails. This moisture-advection feedback allows for the existence of
70 two stable states, separated by a saddle-node bifurcation (Zickfeld et al., 2005) (although
71 interestingly, the conceptual models of Levermann et al. (2009) and Schewe et al. (2012)
72 are characterised by a single bifurcation point for switching ‘off’ the monsoon and an
73 arbitrary threshold to switch it back ‘on’). Crucially, the presence of a critical threshold at
74 the transition between the strong and weak regimes of the EASM means that early warning

75 signals related to ‘critical slowing down’ (Dakos et al., 2008; Lenton et al., 2012) could be
76 detectable in suitable proxy records.

77

78 The aim of this study was twofold: (1) to test whether shifts in the EASM during the
79 penultimate glacial cycle (Marine Isotope Stage 6) are consistent with bifurcational tipping
80 points, and (2) if so, is it possible to detect associated early warning signals. To achieve
81 this, we analyse two $\delta^{18}\text{O}$ speleothem records from China, and construct a simple model
82 that we derive directly from this data to test whether we can detect early warning signals of
83 these transitions.

84

85 **Detecting early warning signals**

86 We perform ‘tipping point analysis’ on both the $\delta^{18}\text{O}$ speleothem records and on multiple
87 simulations derived from our model. This analysis aims to find early warning signs of
88 impending tipping points that are characterised by a bifurcation (rather than a noise-induced
89 or rate-induced tipping e.g. Ashwin et al. (2012)). These tipping points can be
90 mathematically detected by looking at the pattern of fluctuations in the short-term trends of
91 a time-series before the transition takes place. A phenomenon called ‘critical slowing down’
92 occurs on the approach to a tipping point, whereby the system takes longer to recover from
93 small perturbations (Dakos et al., 2008; Held and Kleinen, 2004; Kleinen et al., 2003). This
94 longer recovery rate causes the intrinsic rates of change in the system to decrease, which is
95 detected as a short-term increase in the autocorrelation or ‘memory’ of the time-series (Ives,
96 1995), often accompanied by an increasing trend in variance (Lenton et al., 2012). While it
97 has been theoretically established that autocorrelation and variance should both increase
98 together (Ditlevsen and Johnsen, 2010; Thompson and Sieber, 2011), there are some factors
99 which can negate this, discussed in detail in Dakos et al. (2012b, 2014). Importantly, it is

100 the increasing trend, rather than the absolute values of the autocorrelation and variance that
101 indicate critical slowing down. Detecting the phenomenon of critical slowing down relies
102 on a timescale separation, whereby the timescale forcing the system is much slower than the
103 timescale of the system's internal dynamics, which is in turn much longer than the
104 frequency of data sampling the system (Held and Kleinen, 2004).

105

106 **Missed alarms**

107 Although efforts have been taken to reduce the chances of type I and type II errors by
108 correct pre-processing of data e.g. (Lenton, 2011), totally eradicating the chances of false
109 positive and false negative results remains a challenge (Dakos et al., 2014; Lenton et al.,
110 2012; Scheffer, 2010). Type II errors or 'missed alarms', as discussed in Lenton (2011),
111 may occur when internal noise levels are such that the system is 'tipped' into a different
112 state prior to reaching the bifurcation point, precluding the detection of early warning
113 signals. Type I errors are potentially easier to guard against by employing strict protocols by
114 which to reject a null hypothesis.

115

116 **Using speleothem $\delta^{18}\text{O}$ data as a proxy of past monsoon strength**

117 Highly-resolved ($\sim 10^2$ years) and precisely dated speleothem records of past monsoonal
118 variability are well placed to test for early warning signals. The use of speleothem-based
119 proxies to reconstruct patterns of palaeo-monsoon changes has increased rapidly over recent
120 decades with the development of efficient sampling and dating techniques. However, there
121 is currently some debate surrounding the climatic interpretation of Chinese speleothem $\delta^{18}\text{O}$
122 records (An et al., 2015), which can be influenced by competing factors that affect isotope
123 fractionation. The oxygen isotopic composition of speleothem calcite is widely used to
124 reconstruct palaeohydrological variations due to the premise that speleothem calcite $\delta^{18}\text{O}$

125 records the stable isotopic content of precipitation, which has been shown to be inversely
126 correlated with precipitation amount (Lee and Swann, 2010; Dansgaard, 1964), a
127 relationship known as the ‘amount effect’. Although the $\delta^{18}\text{O}$ of speleothem calcite in China
128 has traditionally been used as a proxy for the ‘amount effect’ (Cheng et al., 2006, 2009;
129 Wang, 2009; Wang et al., 2008), this has been challenged by other palaeo-wetness proxies,
130 notably Maher (2008), who argues that speleothems may be influenced by changes in
131 rainfall source rather than amount. The influence of the Indian Monsoon has also been
132 proposed as an alternative cause for abrupt monsoon variations in China (Liu et al., 2006;
133 Pausata et al., 2011), though this has since been disputed (Liu et al., 2014; Wang and Chen,
134 2012). Importantly, however, robust replications of the same $\delta^{18}\text{O}$ trends in speleothem
135 records across the wider region suggest they principally represent changes in the delivery of
136 precipitation $\delta^{18}\text{O}$ associated with the EASM (Baker et al., 2015; Cheng et al., 2009, 2012;
137 Duan et al., 2014; Li et al., 2013; Liu et al., 2014).

138

139 Specific data requirements are necessary to search for early warning signs of tipping points
140 in climate systems; not only does the data have to represent a measure of climate, it also
141 must be of a sufficient length and resolution to enable the detection of critical slowing
142 down. In addition, since time series analysis methods require interpolation to equidistant
143 data points, a relative constant density of data points is important, so that the interpolation
144 does not skew the data. The speleothem $\delta^{18}\text{O}$ records that we have selected fulfil these
145 criteria, as described in more detail in section 2.1.

146

147

148 **2. Methods**

149 **2.1 Data selection**

150 We used the Chinese speleothem sequences from Sanbao Cave (31°40'N, 110°26'E) (Wang
151 et al., 2008), and Hulu Cave (32°30'N, 119°10'E) (Wang et al., 2001) to search for early
152 warning signals. Sanbao Cave (speleothem SB11) and Hulu Cave (speleothem MSP) have
153 two of the highest resolution chronologies in the time period of interest, with a relatively
154 constant density of data points, providing some of the best records of Quaternary-scale
155 monsoonal variation. Speleothem $\delta^{18}\text{O}$ offer considerable advantages for investigating past
156 changes in the EASM: their long duration (10^3 - 10^4 years), high-resolution (~ 100 years) and
157 precise and absolute-dated chronologies (typically 1 kyr at 1σ), make them ideal for time
158 series analysis. Speleothem SB11 has one of the longest, continuous $\delta^{18}\text{O}$ records in China,
159 and is the only series spanning an entire glacial cycle without using a spliced record (Wang
160 et al. 2008). Speleothem MSP has a comparable resolution and density to SB11, though is
161 significantly shorter. Crucially, the cave systems lie within two regionally distinct areas
162 (Figure 2), indicating that parallel changes in $\delta^{18}\text{O}$ cannot be explained by local effects.

163

164

165 **Figure 2** Map showing the location of Sanbao and Hulu caves.

166

167

168 **2.2 Searching for bimodality**

169 A visual inspection of a histogram of the speleothem $\delta^{18}\text{O}$ data was initially undertaken to
170 determine whether the data are likely to be bimodal. We then applied a Dip-test of
171 unimodality (Hartigan and Hartigan, 1985) to test whether our data is bimodal. To
172 investigate further the dynamical origin of the modality of our data we applied non-
173 stationary potential analysis (Kwasniok, 2013). A non-stationary potential model (discussed
174 in more detail in section 2.4) was fitted, modulated by the solar forcing (NHSI June

175 30°N), covering the possibility of directly forced transitions as well as noise-induced
176 transitions with or without stochastic resonance.

177

178

179 **2.3 Tipping point analysis**

180 A search for early warning signals of a bifurcation at each monsoon transition was carried
181 out between 224-128 ka BP of the Sanbao Cave and Hulu Cave speleothem records. Stable
182 periods of the Sanbao Cave $\delta^{18}\text{O}$ record (e.g. excluding the abrupt transitions) were initially
183 identified visually and confirmed by subsequent analysis using a climate regime shift
184 detection method described by Rodionov (2004). Data pre-processing involved removal of
185 long term trends using a Gaussian kernel smoothing filter and interpolation to ensure that
186 the data is equidistant (a necessary assumption for time-series analysis), before the trends in
187 autocorrelation and variance (using the R functions *acf()* and *var()* respectively) are
188 measured over a sliding window of half the data length (Lenton et al., 2012). The density of
189 data points over time do not change significantly over either record and thus the observed
190 trends in autocorrelation are not an artefact of the data interpolation. The smoothing
191 bandwidth was chosen such that long-term trends were removed, without overfitting the
192 data. A sensitivity analysis was undertaken by varying the size of the smoothing bandwidth
193 and sliding window to ensure the results were robust over a range of parameter choices. The
194 nonparametric Kendall's tau rank correlation coefficient was applied (Dakos et al., 2008;
195 Kendall, 1948) to test for statistical dependence for a sequence of measurements against
196 time, varying between +1 and -1, describing the sign and strength of any trends in
197 autocorrelation and variance.

198

199 **2.3.1 Assessing significance**

200 The results were tested against surrogate time series to ascertain the significance level of the
201 results found, based on the null hypothesis that the data are generated by a stationary
202 Gaussian linear stochastic process. This method for assessing significance of the results is
203 based on Dakos et al. (2012a). The surrogate time series were generated by randomising the
204 original data over 1000 permutations, which is sufficient to adequately estimate the
205 probability distribution of the null model, and destroys the memory while retaining the
206 amplitude distribution of the original time series. The autocorrelation and variance for the
207 original and each of the surrogate time series was computed, and the statistical significance
208 obtained for the original data by comparing against the frequency distribution of the trend
209 statistic (Kendall tau values of autocorrelation and variance) from the surrogate data. The
210 90th and 95th percentiles provided the 90% and 95% rejection thresholds (or p-values of 0.1
211 and 0.05) respectively. According to the fluctuation-dissipation theorem (Ditlevsen and
212 Johnsen, 2010), both autocorrelation and variance should increase together on the approach
213 to a bifurcation. Previous tipping point literature has often used a visual increasing trend of
214 autocorrelation and variance as indicators of critical slowing down. Although using
215 surrogate data allows a quantitative assessment of the significance of the results, there is no
216 consensus on what significance level is necessary to declare the presence of precursors
217 of critical slowing down. To guard against type I errors, we determine for this study that
218 ‘statistically significant’ early warning indicators occur with increases in both
219 autocorrelation and variance with p-values > 0.1 .

220

221 **2.4 Non-stationary potential analysis**

222 To supplement the analysis of the speleothem records and help interpret the results, a simple
223 stochastic model derived directly from this data was constructed. Non-stationary potential
224 analysis (Kwasniok, 2013, 2015) is a method for deriving from time series data a simple

225 dynamical model which is modulated by external factors, here solar insolation. The
 226 technique allows extraction of basic dynamical mechanisms and to distinguish between
 227 competing dynamical explanations.

228

229 The dynamics of the monsoon system are conceptually described as motion in a time-
 230 dependent one-dimensional potential landscape; the influence of unresolved spatial and
 231 tem- poral scales is accounted for by stochastic noise. The governing equation is a one-
 232 dimensional non-stationary effective Langevin equation:

$$233 \quad \dot{x} = -V'(x; t) + \sigma\eta \quad (1)$$

234 η is a white Gaussian noise process with zero mean and unit variance, and σ is the
 235 amplitude of the stochastic forcing. The potential landscape is time-dependent, modulated
 236 by the solar insolation:

$$237 \quad V(x; t) = U(x) + \gamma I(t)x \quad (2)$$

238 The time-independent part of the potential is modelled by a fourth-order polynomial,
 239 allowing for possible bi-stability (Kwasniok and Lohmann, 2009):

$$240 \quad U(x) = \sum_{i=1}^4 a_i x^i \quad (3)$$

241 $I(t)$ is the insolation forcing and γ is a coupling parameter. The modulation of the potential
 242 is only in the linear term, that is, the time-independent potential system is subject to the
 243 scaled insolation forcing $\gamma I(t)$. The model variable x is identified with the speleothem
 244 record. The insolation is represented as a superposition of three main frequencies as

$$245 \quad I(t) = \alpha_0 + \sum_{i=1}^3 [\alpha_i \cos(2\pi t/T_i) + \beta_i \sin(2\pi t/T_i)] \quad (4)$$

246 with time t measured in ky. The expansion coefficients α_i and β_i are determined by least-
 247 squares regression on the insolation time series over the time interval of the speleothem

248 record. The periods T_i are found by a search over a grid with mesh size 0.5ky. They are, in
 249 order of decreasing contribution $\alpha_i^2 + \beta_i^2$, $T_1 = 23\text{ky}$, $T_2 = 19.5\text{ky}$ and $T_3 = 42\text{ky}$. This yields
 250 an excellent approximation of the insolation time series over the time interval under
 251 consideration here.

252

253 The potential model incorporates and allows to distinguish between two possible scenarios:

254 (i) In the bifurcation scenario, the monsoon transitions are directly forced by the insolation.

255 Two states are stable in turn, one at a time. (ii) Alternatively, two stable states could be

256 available at all times with noise-induced switching between them. The height of the

257 potential barrier separating the two states would be modulated by the insolation, possibly

258 giving rise to a stochastic resonance which would explain the high degree of coherence

259 between the solar forcing and the monsoon transitions.

260

261 The shape of the potential, as well as the noise level, are estimated from the data according

262 to the maximum likelihood principle. We take a two-step approach, combining non-

263 stationary probability density modelling (Kwasniok, 2013) and dynamical modeling

264 (Kwasniok, 2015). The shape of the potential is estimated from the probability density of

265 the data. The quasi-stationary probability density of the potential model is

$$266 \quad p(x; t) = Z^{-1}(t) \exp[-2V(x; t)/\sigma^2] \quad (5)$$

267 with a time-dependent normalisation constant $Z(t)$. The coefficients a_i and the coupling

268 constant γ are estimated by maximising the likelihood function

$$269 \quad L(x_1, \dots, x_N) = \prod_{i=1}^N p(x_n; t_n) \quad (6)$$

270 as described in Kwasniok (2013). The size of the data set is N . This leaves the noise level

271 undetermined as a scaling of the potential with a constant c and a simultaneous scaling of

272 the noise variance with c keeps the quasi-stationary probability density unchanged. We set
 273 $\sigma = I$ for the (preliminary) estimation of a_i and γ . The noise level is now determined from
 274 the dynamical likelihood function based on the time evolution of the system (Kwasniok,
 275 2015). The Langevin equation is discretised according to the Euler-Maruyama scheme:

$$x_{n+1} = x_n - \delta t_n V'(x_n; t_n) + \sqrt{\delta t_n} \sigma \eta_n \quad (7)$$

276
 277 The sampling interval of the data is $\delta t_n = t_{n+1} - t_n$. The log-likelihood function of the
 278 data is

$$l(x_1, \dots, x_N | x_0) = -\frac{N}{2} \log 2\pi - N \log \sigma - \sum_{n=0}^{N-1} \frac{1}{2} \log \delta t_n + \frac{1}{2} \frac{[x_{n+1} - x_n + \delta t_n V'(x_n; t_n)]^2}{\delta t_n \sigma^2} \quad (8)$$

279
 280 The scaling constant c is searched on a grid with mesh size 0.01 and the log-likelihood
 281 maximised, giving the final estimates of all parameters. Both estimation procedures are
 282 applied directly to the unevenly sampled data without any prior interpolation. We remark
 283 that the more natural and simpler approach of estimating all parameters simultaneously
 284 from the dynamical likelihood (Kwasniok, 2015) here yields a negative leading-order
 285 coefficient a_4 and thus the model cannot be integrated over a longer time period without the
 286 trajectory escaping to infinity. This possibly points at limitations in the degree of validity of
 287 the one- dimensional potential model. Palaeoclimatic records reflect a multitude of complex
 288 processes and any model as simple as eq.(1) cannot be expected to be more than a crude
 289 skeleton model. The described estimation method guarantees a positive leading-order
 290 coefficient a_4 and therefore a globally stable model.

291

292 It has been suggested that the EASM system responds specifically to 65°N 21st July
 293 insolation with a “near-zero phase lag” (Ruddiman, 2006). However, given that EASM
 294 development is affected by both remote and local insolation forcing (Liu et al., 2006), we
 295 use an insolation latitude local to the Sanbao Cave record, consistent with earlier studies

296 from this and other speleothem sequences (Wang et al., 2001). Since the monthly maximum
297 insolation shifts in time with respect to the precession parameter, the 30°N June insolation
298 was used, though we acknowledge that the insolation changes of 65°N 21 July as used by
299 Wang et al. (2008) are similar with regard to the timing of maxima and minima. Crucially,
300 immediately prior to Termination II, the Chinese speleothem data (including Sanbao Cave)
301 record a ‘Weak Monsoon Interval’ between 135.5 and 129 ka BP (Cheng et al., 2009),
302 suggesting a lag of approximately 6.5 kyrs following Northern Hemisphere summer
303 insolation (Figure 1).

304

305 Having derived a model from the data, 100 realisations were analysed to test whether early
306 warning signals could be detected in the model output, using the methods set out in section
307 2.3. We initially chose the sampling resolution of the model outputs to be comparable to the
308 speleothem data (10^2 years). Sampling the same time series at different resolutions and
309 noise levels allows us to explore the effect of these on the early warning signals.

310 Accordingly, the model was manipulated by changing both the noise level and sampling
311 resolution. To enable a straightforward comparison of the rate of forcing and the sampling
312 resolution we linearized the solar insolation using the minimum and maximum values of the
313 solar insolation over the time span of the model (224-128 ka BP). This approach was
314 preferred rather than using a sinusoidal forcing since early warning signals are known to
315 work most effectively when there is a constant increase in the forcing. To detrend the time
316 series data, we ran the model without any external noise forcing to obtain the equilibrium
317 solution to the system, which we then subtracted from the time series, which did include
318 noise. In addition, we manipulated the noise level of the model by altering the amplitude of
319 the stochastic forcing (σ in Equation 1). The time step in the series was reduced so that
320 6000 time points were available prior to the bifurcation and to ensure no data from beyond

321 the tipping point was included in the analysis. Sampling the same time series at different
322 resolutions allowed us to explore the effect of this on the early warning signals. When
323 comparing early warning signals for differing sample steps and noise levels, the same
324 iteration of the model was used to enable a direct comparison.

325

326 **3. Results**

327 **3.1 Searching for bimodality**

328 A histogram of $\delta^{18}\text{O}$ values suggests that there are two modes in the EASM between 224-
329 128 ka BP, as displayed by the double peak structure in Figure 3a, supporting a number of
330 studies that observe bimodality in tropical monsoon systems (Schewe et al., 2012; Zickfeld
331 et al., 2005). We also apply a Dip-test of unimodality (Hartigan and Hartigan, 1985) and
332 find that our null hypothesis of unimodality is rejected ($D=0.018$, $p=0.0063$) and thus our
333 data is at least bimodal. To investigate further the dynamical origin of this bimodality we
334 applied non-stationary potential analysis (Kwasniok, 2013). This showed a bi-stable
335 structure to the EASM with hysteresis (Figure 3b, c), suggesting that abrupt monsoon
336 transitions may involve underlying bifurcations. The monsoon transitions appear to be
337 predominantly directly forced by the insolation. There is a phase in the middle of the
338 transition cycle between the extrema of the insolation where two stable states are available
339 at the same time but this phase is too short for noise-induced switches to play a significant
340 role.

341

342

343 **Figure 3** (a) Histogram showing the probability density of the speleothem data aggregated
344 over 224-128 ka BP, (b) Bifurcation diagram obtained from potential model analysis,
345 showing bi-stability and hysteresis. Solid black lines indicate stable states, dotted line

346 unstable states, and dashed vertical lines the jumps between the two stable branches.
347 Coloured vertical lines correspond to the insolation values for which the potential curve is
348 shown in panel c; (c) Shows how the shape of the potential well changes over one transition
349 cycle (198-175 ka BP) (green long dash = 535 W/m², purple short dash = 531 W/m², blue
350 solid = 490 W/m², red dotted = 449 W/m²) (for more details see Figure 10).

351

352

353 **3.2 Tipping point analysis**

354 We applied tipping point analysis on the Sanbao Cave $\delta^{18}\text{O}$ record on each section of data
355 prior to a monsoon transition. Although autocorrelation and variance do increase prior to
356 some of the abrupt monsoon transitions (Figure 4), these increases are not consistent
357 through the entire record. Surrogate datasets used to test for significance of our results
358 showed that p-values associated with these increases are never <0.1 for both autocorrelation
359 and variance (Figure 5). Although a visual increasing trend has been used in previous
360 literature as an indicator of critical slowing down, we choose more selective criteria to
361 guard against the possibility of false positives.

362

363

364 **Figure 4** a) $\delta^{18}\text{O}$ speleothem data from Sanbao Cave (SB11) (blue line) and NHSI at July
365 65°N (grey line). Grey hatched areas show the sections of data selected for tipping point
366 analysis. b) These panels show the corresponding autocorrelation and variance for each
367 period prior to a transition.

368

369

370 **Figure 5** Histogram showing frequency distribution of Kendall tau values from 1000
371 realisations of a surrogate time series model, for Sanbao Cave (a, b) and Hulu Cave (c, d)
372 $\delta^{18}\text{O}$ data. The grey dashed lines indicate the 90% and 95% significance level and the blue
373 and red vertical lines show the Kendall tau values for autocorrelation and variance, for each
374 section of speleothem data analysed. The blue circle in (a) and the red circle in (b) indicate
375 the Kendall tau values for the section of data spanning the period 150 to 129 ka BP
376 immediately prior to Termination II.

377

378

379 The only section of data prior to a monsoon transition that sees p-values of <0.1 for the
380 increases in both autocorrelation and variance is for the data spanning the period 150 to 129
381 ka BP in the Sanbao Cave record, before Monsoon Termination II (Figure 6). We find that
382 the Kendall tau value for autocorrelation has a significance level of $p < 0.05$ and for
383 variance a significance level of $p < 0.1$ (Figure 5a and 5b). These proportional positive
384 trends in both autocorrelation and variance are consistent with critical slowing down on the
385 approach to a bifurcation (Ditlevsen and Johnsen, 2010). Figure 6c illustrates the density of
386 data points before and after interpolation, showing that this pre-processing is unlikely to
387 have biased the results.

388

389

390 **Figure 6** Tipping Point analysis on data from Sanbao Cave (Speleothem SB11) ($31^{\circ}40'\text{N}$,
391 $110^{\circ}26'\text{E}$). (a) Data was smoothed over an appropriate bandwidth (purple line) to produce
392 data residuals (b), and analysed over a sliding window (of size between the two grey
393 vertical lines). The grey vertical line at 131 ka BP indicates the tipping point, and the point
394 up to which the data is analysed. (c,d) Data density, where the black points are the original

395 data and the pink points are the data after interpolation. (e) AR(1) values and associated
396 Kendall tau value, and (f) displays the variance and associated Kendall tau.

397

398 To test whether the signal is present in other EASM records, we undertook the same
399 analysis on a second speleothem sequence (Figure 7), covering the same time period. We
400 find that speleothem MSP from Hulu Cave (32°30'N, 119°10'E) (Wang et al., 2001)
401 displays a comparable increase in autocorrelation and variance to speleothem SB11 from
402 Sanbao Cave, though these do display slightly lower p-values; see Figure 5c and 5d.

403

404

405 **Figure 7** Tipping Point analysis on data from Hulu Cave (Speleothem MSP) (32°30' N,
406 119°10' E) (a) Data was smoothed over an appropriate bandwidth (purple line) to produce
407 data residuals (b), and analysed over a sliding window (of size between the two grey
408 vertical lines). The grey vertical line at 131 kaBP indicates the tipping point, and the point
409 up to which the data is analysed. (c, d) Data density, where the black points are the original
410 data and the pink points are the data after interpolation. (e) Autocorrelation values and
411 associated Kendall tau value, and (f) the variance and associated Kendall tau.

412

413

414 Furthermore, a sensitivity analysis was performed (results shown for data preceding the
415 monsoon termination in both speleothem SB11 and MSP, Figure 8) to ensure that the results
416 were robust over a range of parameters by running repeats of the analysis with a range of
417 smoothing bandwidths used to detrend the original data (5-15% of the time series length)
418 and sliding window sizes in which indicators are estimated (25-75% of the time series
419 length). The colour contours show how the Kendall tau values change when using different

420 parameter choices; for the autocorrelation at Sanbao Cave the Kendall tau values are over
421 0.8 for the vast majority of smoothing bandwidth and sliding window sizes (Figure 8a),
422 indicating a robust analysis.

423

424

425 **Figure 8** Contour plots showing a range of window and bandwidth sizes for the analysis;
426 (a) Sanbao SB11 autocorrelation, (b) Sanbao SB11 variance, (c) Hulu MSP autocorrelation,
427 (d) Hulu MSP variance. Black stars indicate the parameters used for the analysis in Figures
428 6 and 7.

429

430

431 **3.3 Non-stationary potential analysis**

432 To help interpret these results we applied our potential model. In the model we find
433 transitions occur under direct solar insolation forcing when reaching the end of the stable
434 branches, explaining the high degree of synchronicity between the transitions and solar
435 forcing. The initial 100 realisations produced from our potential model appear broadly to
436 follow the path of June insolation at 30°N with a small phase lag (Figure 9). The model
437 simulations also follow the speleothem palaeodata for all but the monsoon transition at 129
438 ka BP near Termination II, where the model simulations show no extended lag with respect
439 to the insolation.

440

441

442 **Figure 9** Probability range of 100 model simulations, with the June 30°N NHSI (in red),
443 and the palaeodata from SB11 (in green)

444

445

446 No consistent early warning signals were found in the initial 100 model simulations during
447 the period 224-128 ka BP. In order to detect critical slowing down on the approach to a
448 bifurcation, the data must capture the gradual flattening of the potential well. We suggest
449 that early warning signals were not detected due to a relatively fast rate of forcing compared
450 to the sampling of the system; this comparatively poor sampling prevents the gradual
451 flattening of the potential well from being recorded in the data; a feature common to many
452 palaeoclimate datasets. Figure 10 illustrates the different flattening of the potential well
453 over a normal transition cycle and over the transition cycle at the termination. There is more
454 visible flattening in the potential at the termination, as seen in panel (c), which is thought to
455 be due to the reduced amplitude of the solar forcing at the termination.

456

457

458 **Figure 10** Potential analysis showing the changing shape of the potential well over (b) a
459 normal transition cycle; and (c) the transition cycle at the termination. (Dotted lines show
460 stages of the transition over high, medium, and low insolation values).

461

462

463 To test the effect on the early warning signals of the sampling resolution of the model, we
464 compared a range of different sampling time steps in the model (see section 2.4) measuring
465 the Kendall tau values of autocorrelation and variance over each realisation of the model
466 (one realisation displayed in Figure 11), which demonstrates the effects of increasing the
467 sampling time step in the model. We found that whereas an increasing sampling time step
468 produces a steady decrease in the Kendall tau values for autocorrelation (Figure 11b),
469 Kendall tau values remain fairly constant for variance (Figure 11c), suggesting that the

470 latter is not affected by time step changes. This supports the contention by Dakos et al.
471 (2012b) that ‘high resolution sampling has no effect on the estimate of variance’. In
472 addition, we manipulated the noise level and found that decreasing the noise level by a
473 factor of 2 was necessary to identify consistent early warning signals. This is illustrated in
474 Figure 11a, where the grey line represents the noise level as determined by the model,
475 which does not follow a step transition, and cannot be adequately detrended by the equation
476 derived from the model. However, once the noise level is sufficiently reduced, early
477 warning signals (displayed here as high Kendall tau values for autocorrelation and variance)
478 can be detected.

479

480

481 **Figure 11** a) Example of single realisation of the approach to a bifurcation over 4 noise
482 levels (original noise = grey, 0.5 noise = black, 0.2 noise = blue, 0.1 noise = green), the red
483 line is the detrending line and the grey dashed vertical line is the cut-off point where data is
484 analysed up to; b) distribution of Kendall tau values for autocorrelation over increasing
485 sample step; c) distribution of Kendall tau values for variance over increasing sample step.

486

487

488 **4. Discussion**

489 It is important to note here that although the detection of early warning signals in time series
490 data has been widely used for the detection of bifurcations in a range of systems (Dakos et
491 al., 2008), there are instances when critical slowing down cannot be detected/recorded prior
492 to a bifurcation. This can be due to external dynamics of the system, such as a high level of
493 stochastic noise, or when there is an insufficient sampling resolution. These results confirm
494 that early warning signals may not be detected for bifurcations if the rate of forcing is too

495 fast compared to the sampling rate, such that the flattening of the potential is poorly
496 recorded in time series. ‘Missed alarms’ may therefore be common in palaeodata where
497 there is an insufficient sampling resolution to detect the flattening of the potential; a high
498 sampling resolution is thus recommended to avoid this issue. There is more flattening
499 visible in the potential for the monsoon transition at 129 ka BP (Termination II) which is
500 due to the reduced amplitude of the solar forcing at the termination, but it is unclear whether
501 this is sufficient to explain the early warning signal detected in the palaeodata. We suggest
502 that additional forcing mechanisms may be driving the termination e.g. (Caley et al., 2011)
503 which cannot be captured by the potential model (as evidenced by the trajectory of the data
504 falling outside the probability range of the potential model (Figure 9)).

505

506 One possible reason for the detection of a critical slowing down immediately prior to the
507 termination (129 ka BP) is a change in the background state of the climate system.
508 Termination II is preceded by a Weak Monsoon Interval (WMI) in the EASM at 135.5-129
509 ka BP (Cheng et al., 2009), characterised by the presence of a longer lag between the
510 change in insolation and the monsoon transition. The WMI is thought to be linked to
511 migrations in the Inter-tropical Convergence Zone (ITCZ) (Yancheva et al., 2007). Changes
512 in the latitudinal temperature gradient (Rind, 1998) or planetary wave patterns (Wunsch,
513 2006) driven by continental ice volume (Cheng et al., 2009) and/or sea ice extent (Broccoli
514 et al., 2006) have been suggested to play a role in causing this shift in the ITCZ. For
515 instance, the cold anomaly associated with Heinrich event 11 (at 135 ka BP) has been
516 invoked as a possible cause of the WMI, cooling the North Atlantic and shifting the Polar
517 Front and Siberian High southwards, forcing an equatorward migration of westerly airflow
518 across Asia (Broecker et al., 1985; Cai et al., 2015; Cheng et al., 2009). Such a scenario
519 would have maintained a low thermal gradient between the land and sea, causing the Weak

520 Monsoon Interval and potentially suppressing a simple insolation response. The implication
521 is that during the earlier monsoon transitions in Stage 6, continental ice volume and/or sea-
522 ice extent was less extensive than during the WMI, allowing the solar insolation response to
523 dominate.

524

525

526 **5. Conclusions**

527 We analysed two speleothem $\delta^{18}\text{O}$ records from China over the penultimate glacial cycle as
528 proxies for the past strength of the EASM to test whether we could detect early warning
529 signals of the transitions between the strong and weak regimes. After determining that the
530 data was bimodal, we derived a non-stationary potential model directly from this data
531 featuring a fold bifurcation structure. We found evidence of critical slowing down before
532 the abrupt monsoon shift at Termination II (129 ka BP) in the speleothem $\delta^{18}\text{O}$ data.

533 However, we do not find consistent early warning signals of a bifurcation for the abrupt
534 monsoon shifts in the period between 224-150 ka BP, which we term ‘missed alarms’.

535 Exploration of sampling resolution from our model suggests that the absence of robust
536 critical slowing down signals in the palaeodata is due to a combination of rapid forcing and
537 the insufficient sampling resolution, preventing the detection of the steady flattening of the
538 potential that occurs before a bifurcation. We also find that there is a noise threshold at
539 which early warning signals can no longer be detected. We suggest that the early warning
540 signal detected at Termination II in the palaeodata is likely due to the longer lag during the
541 Weak Monsoon Interval, linked to cooling in the North Atlantic. This allows a steadier
542 flattening of the potential associated with the stability of the EASM and thus enables the
543 detection of critical slowing down. Our results have important implications for identifying
544 early warning signals in other natural archives, including the importance of sampling

545 resolution and the background state of the climate system (full glacial versus termination).
546 In addition, it is advantageous to use archives which record multiple transitions, rather than
547 a single shift, such as the speleothem records reported here; the detection of an early
548 warning signal during one transition compared to previous events in the same record
549 provides an insight into changing/additional forcing mechanisms.

550

551

552

553 **References**

554 An, Z.: The history and variability of the East Asian paleomonsoon climate, *Quat. Sci. Rev.*,
555 19(1-5), 171–187, doi:10.1016/S0277-3791(99)00060-8, 2000.

556 An, Z., Guoxiong, W., Jianping, L., Youbin, S., Yimin, L., Weijian, Z., Yanjun, C., Anmin,
557 D., Li, L., Jiangyu, M., Hai, C., Zhengguo, S., Liangcheng, T., Hong, Y., Hong, A., Hong,
558 C. and Juan, F.: Global Monsoon Dynamics and Climate Change, *Annu. Rev. Earth Planet.*
559 *Sci.*, 43(2), 1–49, doi:10.1146/annurev-earth-060313-054623, 2015.

560 Ashwin, P., Wieczorek, S., Vitolo, R. and Cox, P.: Tipping points in open systems:
561 bifurcation, noise-induced and rate-dependent examples in the climate system, *Philos.*
562 *Trans. R. Soc. A Math. Phys. Eng. Sci.*, 370, 1–20, 2012.

563 Baker, A. J., Sodemann, H., Baldini, J. U. L., Breitenbach, S. F. M., Johnson, K. R., van
564 Hunen, J. and Pingzhong, Z.: Seasonality of westerly moisture transport in the East Asian
565 Summer Monsoon and its implications for interpreting precipitation $\delta^{18}\text{O}$, *J. Geophys. Res.*
566 *Atmos.*, doi:10.1002/2014JD022919, 2015.

567 Berger, A. and Loutre, M. F.: Insolation values for the climate of the last 10 million years,
568 *Quat. Sci. Rev.*, 10(1988), 297–317, 1991.

569 Broccoli, A. J., Dahl, K. a. and Stouffer, R. J.: Response of the ITCZ to Northern
570 Hemisphere cooling, *Geophys. Res. Lett.*, 33, 1–4, doi:10.1029/2005GL024546, 2006.

571 Broecker, W. S., Peteet, D. M. and Rind, D.: Does the ocean-atmosphere system have more
572 than one stable mode of operation?, *Nature*, 315, 21–26, 1985.

573 Cai, Y., Fung, I. Y., Edwards, R. L., An, Z., Cheng, H., Lee, J.-E., Tan, L., Shen, C.-C.,
574 Wang, X., Day, J. a., Zhou, W., Kelly, M. J. and Chiang, J. C. H.: Variability of stalagmite-
575 inferred Indian monsoon precipitation over the past 252,000 y, *Proc. Natl. Acad. Sci.*,
576 112(10), 2954–2959, doi:10.1073/pnas.1424035112, 2015.

- 577 Caley, T., Malaizé, B., Revel, M., Ducassou, E., Wainer, K., Ibrahim, M., Shoeaib, D.,
578 Migeon, S. and Marieu, V.: Orbital timing of the Indian, East Asian and African boreal
579 monsoons and the concept of a “global monsoon,” *Quat. Sci. Rev.*, 30(25-26), 3705–3715,
580 doi:10.1016/j.quascirev.2011.09.015, 2011.
- 581 Cheng, H., Edwards, R. L., Broecker, W. S., Denton, G. H., Kong, X., Wang, Y., Zhang, R.
582 and Wang, X.: Ice Age Terminations, *Science* (80-.), 326, 248–252,
583 doi:10.1126/science.1177840, 2009.
- 584 Cheng, H., Edwards, R. L., Wang, Y., Kong, X., Ming, Y., Kelly, M. J., Wang, X., Gallup,
585 C. D. and Liu, W.: A penultimate glacial monsoon record from Hulu Cave and two-phase
586 glacial terminations, *Geology*, 34(3), 217, doi:10.1130/G22289.1, 2006.
- 587 Cheng, H., Sinha, A., Wang, X., Cruz, F. W. and Edwards, R. L.: The Global
588 Paleomonsoon as seen through speleothem records from Asia and the Americas, *Clim.*
589 *Dyn.*, 39(5), 1045–1062, doi:10.1007/s00382-012-1363-7, 2012.
- 590 Dakos, V., Carpenter, S. R., Brock, W. A., Ellison, A. M., Guttal, V., Ives, A. R., Kéfi, S.,
591 Livina, V., Seekell, D. A., van Nes, E. H. and Scheffer, M.: Methods for detecting early
592 warnings of critical transitions in time series illustrated using simulated ecological data.,
593 *PLoS One*, 7(7), e41010, doi:10.1371/journal.pone.0041010, 2012a.
- 594 Dakos, V., Carpenter, S. R., van Nes, E. H. and Scheffer, M.: Resilience indicators:
595 prospects and limitations for early warnings of regime shifts, *Philos. Trans. R. Soc. B Biol.*
596 *Sci.*, 370, 20130263, doi:10.1098/rstb.2013.0263, 2014.
- 597 Dakos, V., van Nes, E. H., D’Odorico, P. and Scheffer, M.: Robustness of variance and
598 autocorrelation as indicators of critical slowing down, *Ecology*, 93(2), 264–271, 2012b.
- 599 Dakos, V., Scheffer, M., van Nes, E. H., Brovkin, V., Petoukhov, V. and Held, H.: Slowing
600 down as an early warning signal for abrupt climate change., *Proc. Natl. Acad. Sci. U. S. A.*,
601 105(38), 14308–12, doi:10.1073/pnas.0802430105, 2008.
- 602 Ditlevsen, P. D. and Johnsen, S. J.: Tipping points: Early warning and wishful thinking,
603 *Geophys. Res. Lett.*, 37(19), L19703, doi:10.1029/2010GL044486, 2010.
- 604 Duan, F., Liu, D., Cheng, H., Wang, X., Wang, Y., Kong, X. and Chen, S.: A high-
605 resolution monsoon record of millennial-scale oscillations during Late MIS 3 from Wulu
606 Cave, south-west China, *J. Quat. Sci.*, 29(1), 83–90, doi:10.1002/jqs.2681, 2014.
- 607 Hartigan, J. A. and Hartigan, P. M.: The Dip Test of Unimodality, *Ann. Stat.*, 13(1), 70–84,
608 1985.
- 609 Held, H. and Kleinen, T.: Detection of climate system bifurcations by degenerate
610 fingerprinting, *Geophys. Res. Lett.*, 31(23), L23207, doi:10.1029/2004GL020972, 2004.
- 611 Ives, A.: Measuring Resilience in Stochastic Systems, *Ecol. Monogr.*, 65(2), 217–233,
612 1995.
- 613 Kendall, M. G.: Rank correlation methods., Griffen, Oxford., 1948.

- 614 Kleinen, T., Held, H. and Petschel-Held, G.: The potential role of spectral properties in
615 detecting thresholds in the Earth system: application to the thermohaline circulation, *Ocean*
616 *Dyn.*, 53(2), 53–63, doi:10.1007/s10236-002-0023-6, 2003.
- 617 Kutzbach, J. E.: Monsoon climate of the early Holocene: climate experiment with the
618 Earth's orbital parameters for 9000 years ago, *Science* (80-.), 214(4516), 59–61, 1981.
- 619 Kwasniok, F.: Predicting critical transitions in dynamical systems from time series using
620 nonstationary probability density modeling., *Phys. Rev. E*, 88, 052917,
621 doi:10.1103/PhysRevE.88.052917, 2013.
- 622 Kwasniok, F.: Forecasting critical transitions using data-driven nonstationary dynamical
623 modeling, submitted, 2015.
- 624 Kwasniok, F. and Lohmann, G.: Deriving dynamical models from paleoclimatic records:
625 Application to glacial millennial-scale climate variability, *Phys. Rev. E*, 80(6), 066104,
626 doi:10.1103/PhysRevE.80.066104, 2009.
- 627 Lenton, T. M.: Early warning of climate tipping points, *Nat. Clim. Chang.*, 1(4), 201–209,
628 doi:10.1038/nclimate1143, 2011.
- 629 Lenton, T. M., Livina, V. N., Dakos, V., van Nes, E. H. and Scheffer, M.: Early warning of
630 climate tipping points from critical slowing down: comparing methods to improve
631 robustness, *Philos. Trans. A. Math. Phys. Eng. Sci.*, 370(1962), 1185–204,
632 doi:10.1098/rsta.2011.0304, 2012.
- 633 Levermann, A., Schewe, J., Petoukhov, V. and Held, H.: Basic mechanism for abrupt
634 monsoon transitions., *Proc. Natl. Acad. Sci. U. S. A.*, 106(49), 20572–7,
635 doi:10.1073/pnas.0901414106, 2009.
- 636 Li, T.-Y., Shen, C.-C., Huang, L.-J., Jiang, X.-Y., Yang, X.-L., Mii, H.-S., Lee, S.-Y. and
637 Lo, L.: Variability of the Asian summer monsoon during the penultimate glacial/interglacial
638 period inferred from stalagmite oxygen isotope records from Yangkou cave, Chongqing,
639 Southwestern China, *Clim. Past Discuss.*, 9(6), 6287–6309, doi:10.5194/cpd-9-6287-2013,
640 2013.
- 641 Lisiecki, L. E. and Raymo, M. E.: A Pliocene-Pleistocene stack of 57 globally distributed
642 benthic $\delta^{18}\text{O}$ records, *Paleoceanography*, 20(1), 1–17, doi:10.1029/2004PA001071, 2005.
- 643 Liu, X., Liu, Z., Kutzbach, J. E., Clemens, S. C. and Prell, W. L.: Hemispheric Insolation
644 Forcing of the Indian Ocean and Asian Monsoon: Local versus Remote Impacts, *Am.*
645 *Meteorol. Soc.*, 19, 6195–6208, 2006.
- 646 Liu, Z., Wen, X., Brady, E. C., Otto-Bliesner, B., Yu, G., Lu, H., Cheng, H., Wang, Y.,
647 Zheng, W., Ding, Y., Edwards, R. L., Cheng, J., Liu, W. and Yang, H.: Chinese cave
648 records and the East Asia Summer Monsoon, *Quat. Sci. Rev.*, 83, 115–128,
649 doi:10.1016/j.quascirev.2013.10.021, 2014.

- 650 Maher, B. A.: Holocene variability of the East Asian summer monsoon from Chinese cave
651 records: a re-assessment, *The Holocene*, 18(6), 861–866, doi:10.1177/0959683608095569,
652 2008.
- 653 Pausata, F. S. R., Battisti, D. S., Nisancioglu, K. H. and Bitz, C. M.: Chinese stalagmite
654 $\delta^{18}\text{O}$ controlled by changes in the Indian monsoon during a simulated Heinrich event, *Nat.*
655 *Geosci.*, 4(7), 474–480, doi:10.1038/ngeo1169, 2011.
- 656 Petit, J. R., Raynaud, D., Basile, I., Chappellaz, J., Davisk, M., Ritz, C., Delmotte, M.,
657 Legrand, M., Lorius, C., Pe, L. and Saltzman, E.: Climate and atmospheric history of the
658 past 420,000 years from the Vostok ice core, Antarctica, *Nature*, 399, 429–436, 1999.
- 659 Rind, D.: Latitudinal temperature gradients and climate change, *J. Geophys. Res.*, 103,
660 5943, doi:10.1029/97JD03649, 1998.
- 661 Rodionov, S. N.: A sequential algorithm for testing climate regime shifts, *Geophys. Res.*
662 *Lett.*, 31(9), L09204, doi:10.1029/2004GL019448, 2004.
- 663 Ruddiman, W. F.: What is the timing of orbital-scale monsoon changes?, *Quat. Sci. Rev.*,
664 25(7-8), 657–658, doi:10.1016/j.quascirev.2006.02.004, 2006.
- 665 Scheffer, M.: Foreseeing tipping points, *Nature*, 467, 6–7, 2010.
- 666 Schewe, J., Levermann, A. and Cheng, H.: A critical humidity threshold for monsoon
667 transitions, *Clim. Past*, 8(2), 535–544, doi:10.5194/cp-8-535-2012, 2012.
- 668 Sun, Y., Kutzbach, J., An, Z., Clemens, S., Liu, Z., Liu, W., Liu, X., Shi, Z., Zheng, W.,
669 Liang, L., Yan, Y. and Li, Y.: Astronomical and glacial forcing of East Asian summer
670 monsoon variability, *Quat. Sci. Rev.*, 115(2015), 132–142,
671 doi:10.1016/j.quascirev.2015.03.009, 2015.
- 672 Thompson, J. and Sieber, J.: Predicting climate tipping as a noisy bifurcation: a review, *Int.*
673 *J. Bifurc. Chaos*, 21(2), 399–423, 2011.
- 674 Wang, H. and Chen, H.: Climate control for southeastern China moisture and precipitation:
675 Indian or East Asian monsoon?, *J. Geophys. Res. Atmos.*, 117(D12), D12109,
676 doi:10.1029/2012JD017734, 2012.
- 677 Wang, P.: Global monsoon in a geological perspective, *Chinese Sci. Bull.*, 54(7), 1113–
678 1136, doi:10.1007/s11434-009-0169-4, 2009.
- 679 Wang, Y., Cheng, H., Edwards, R. L., Kong, X., Shao, X., Chen, S., Wu, J., Jiang, X.,
680 Wang, X. and An, Z.: Millennial- and orbital-scale changes in the East Asian monsoon over
681 the past 224,000 years, *Nature*, 451, 18–21, doi:10.1038/nature06692, 2008.
- 682 Wang, Y. J., Cheng, H., Edwards, R. L., An, Z. S., Wu, J. Y., Shen, C. C. and Dorale, J. a:
683 A high-resolution absolute-dated late Pleistocene Monsoon record from Hulu Cave, China.,
684 *Science* (80-.), 294(5550), 2345–8, doi:10.1126/science.1064618, 2001.

- 685 Wu, G., Liu, Y., He, B., Bao, Q., Duan, A. and Jin, F.-F.: Thermal controls on the Asian
686 summer monsoon., *Sci. Rep.*, 2(404), 1–7, doi:10.1038/srep00404, 2012.
- 687 Wunsch, C.: Abrupt climate change: An alternative view, *Quat. Res.*, 65(2006), 191–203,
688 doi:10.1016/j.yqres.2005.10.006, 2006.
- 689 Yancheva, G., Nowaczyk, N. R., Mingram, J., Dulski, P., Schettler, G., Negendank, J. F.
690 W., Liu, J., Sigman, D. M., Peterson, L. C. and Haug, G. H.: Influence of the intertropical
691 convergence zone on the East Asian monsoon., *Nature*, 445(7123), 74–7,
692 doi:10.1038/nature05431, 2007.
- 693 Yuan, D., Cheng, H., Edwards, R. L., Dykoski, C. A., Kelly, M. J., Zhang, M., Qing, J.,
694 Lin, Y., Wang, Y., Wu, J., Dorale, J. A., An, Z. and Cai, Y.: Timing, duration, and
695 transitions of the last interglacial Asian monsoon., *Science (80-.)*, 304(5670), 575–8,
696 doi:10.1126/science.1091220, 2004.
- 697 Zhang, P., Cheng, H., Edwards, R. L., Chen, F., Wang, Y., Yang, X., Liu, J., Tan, M.,
698 Wang, X., Liu, J., An, C., Dai, Z., Zhou, J., Zhang, D., Jia, J., Jin, L. and Johnson, K. R.: A
699 test of climate, sun, and culture relationships from an 1810-year Chinese cave record.,
700 *Science (80-.)*, 322(5903), 940–2, doi:10.1126/science.1163965, 2008.
- 701 Zickfeld, K., Knopf, B., Petoukhov, V. and Schellnhuber, H. J.: Is the Indian summer
702 monsoon stable against global change?, *Geophys. Res. Lett.*, 32(15), L15707,
703 doi:10.1029/2005GL022771, 2005.

704

705 **Acknowledgements**

706 We thank Sue Rouillard from the drawing office in the Geography department at the
707 University of Exeter for drawing Figure 2.

708 The data for this paper are available from the National Climate Data Centre, NOAA (SB11:

709 http://hurricane.ncdc.noaa.gov/pls/paleox/f?p=519:1:::P1_STUDY_ID:8641 and Hulu:

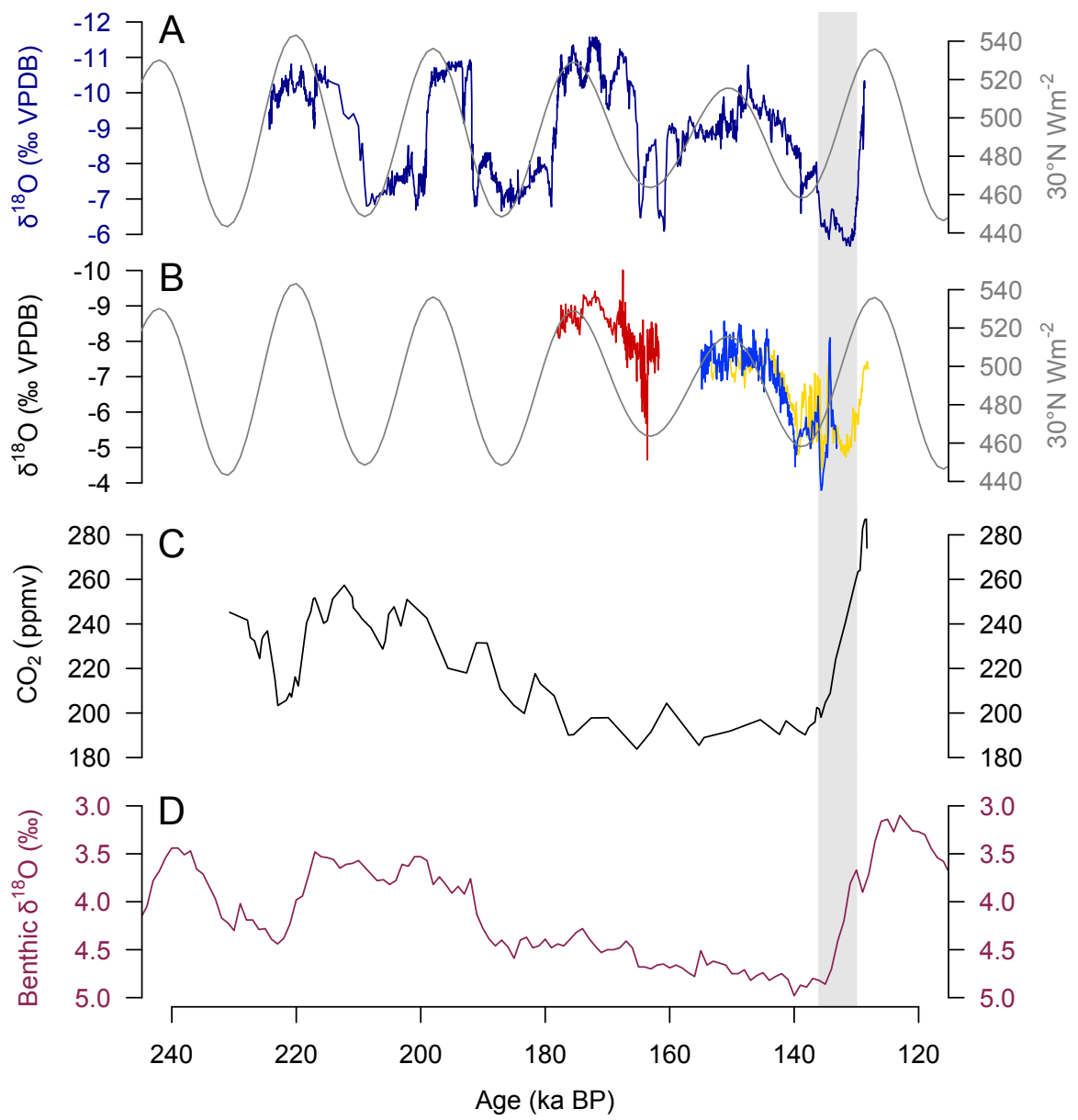
710 http://hurricane.ncdc.noaa.gov/pls/paleox/f?p=519:1:::P1_STUDY_ID:5426)

711

712 **Competing financial interests**

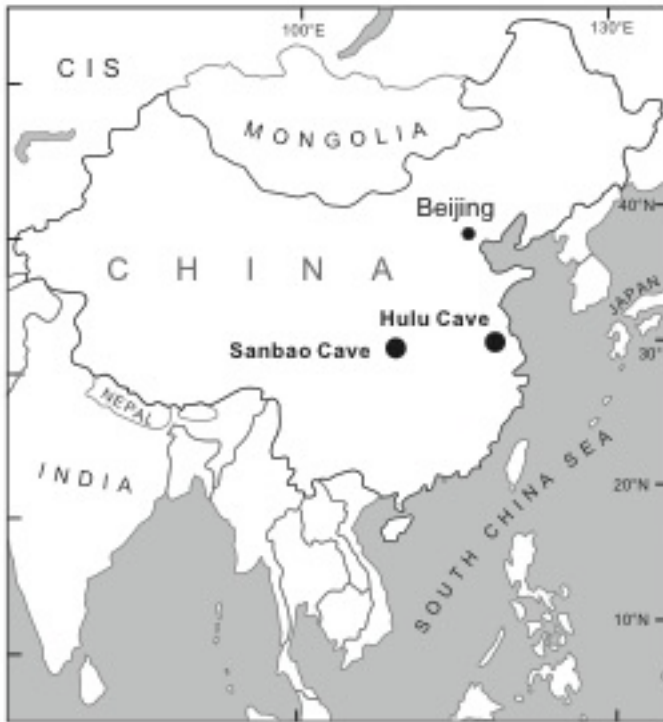
713 The authors declare no competing financial interests.

714



715

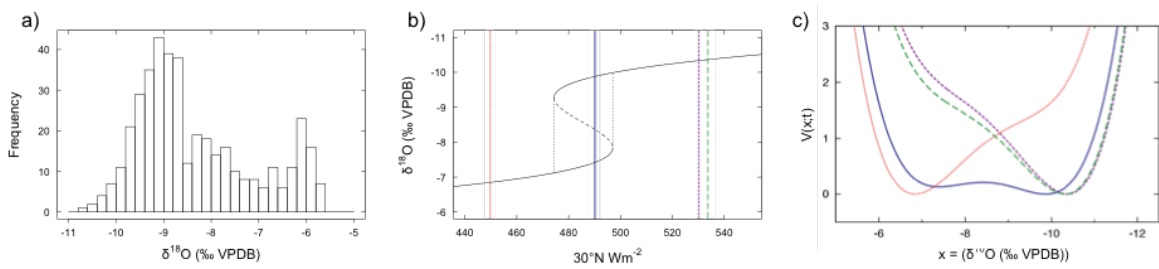
716 (Figure 1)



717

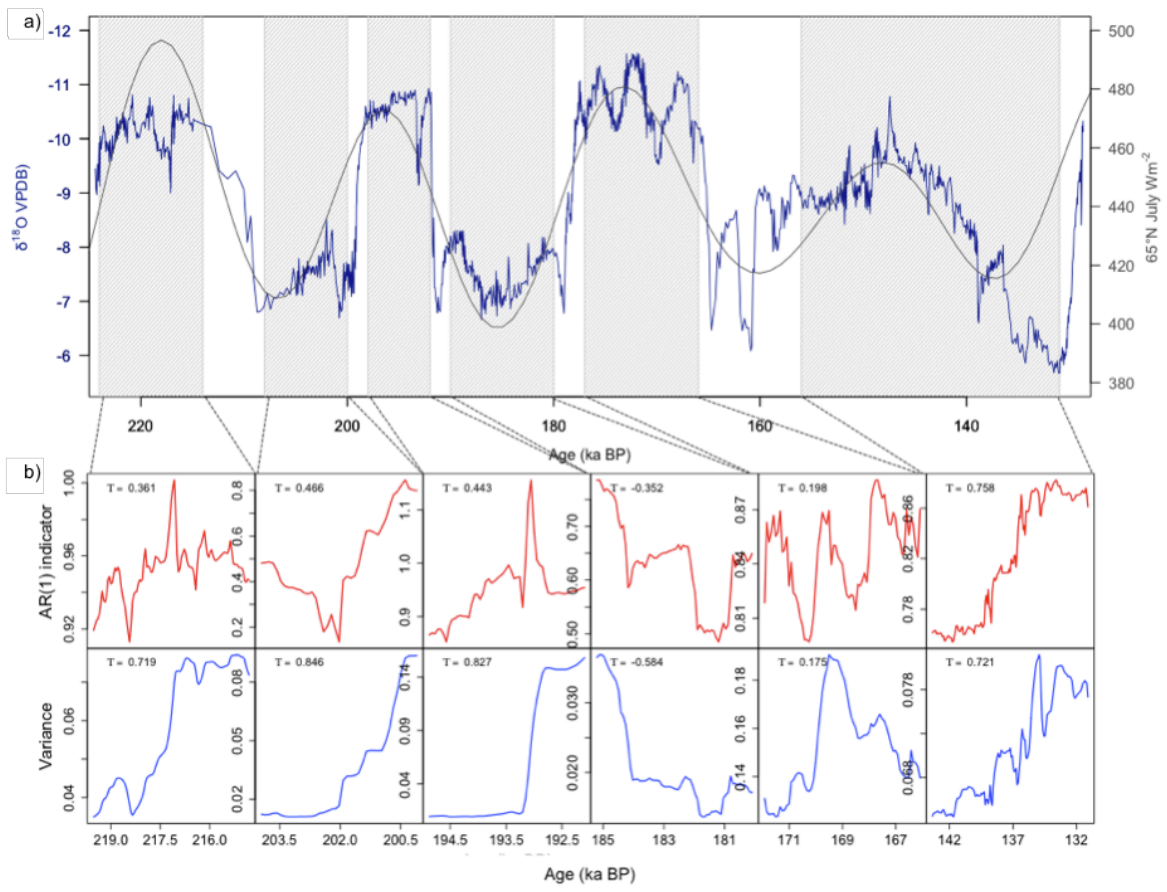
718 (Figure 2)

719



720

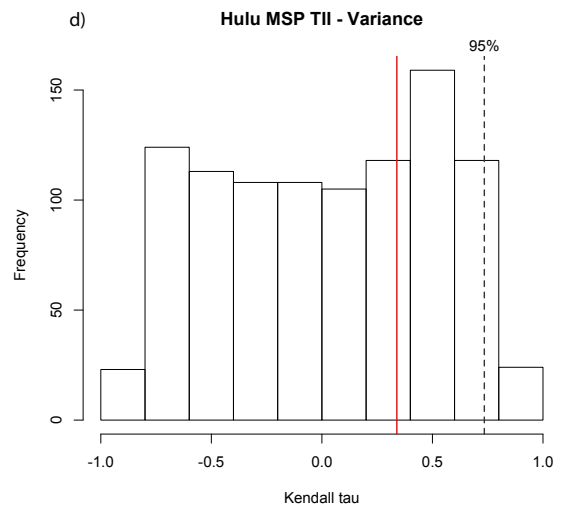
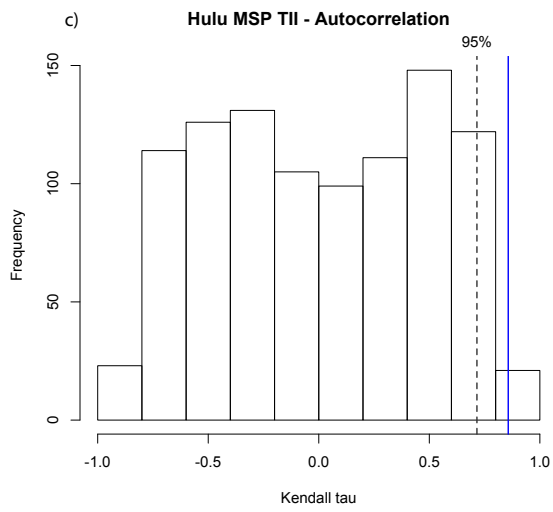
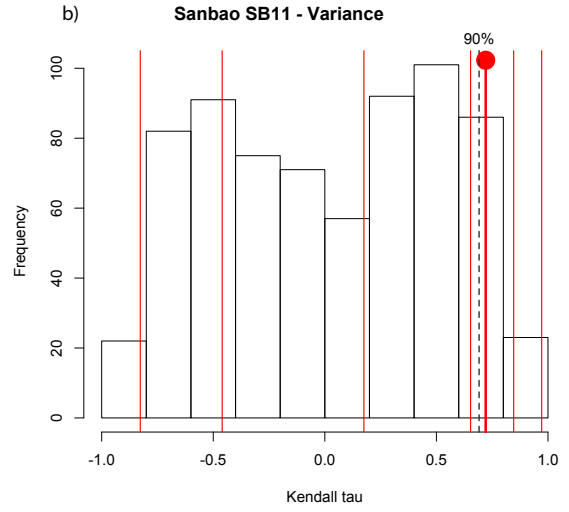
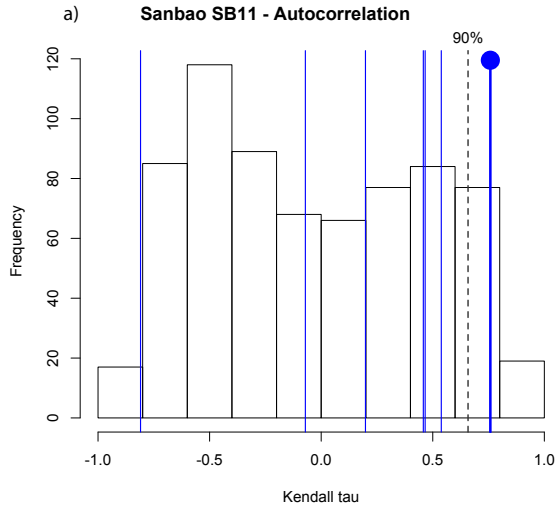
721 (Figure 3)



722

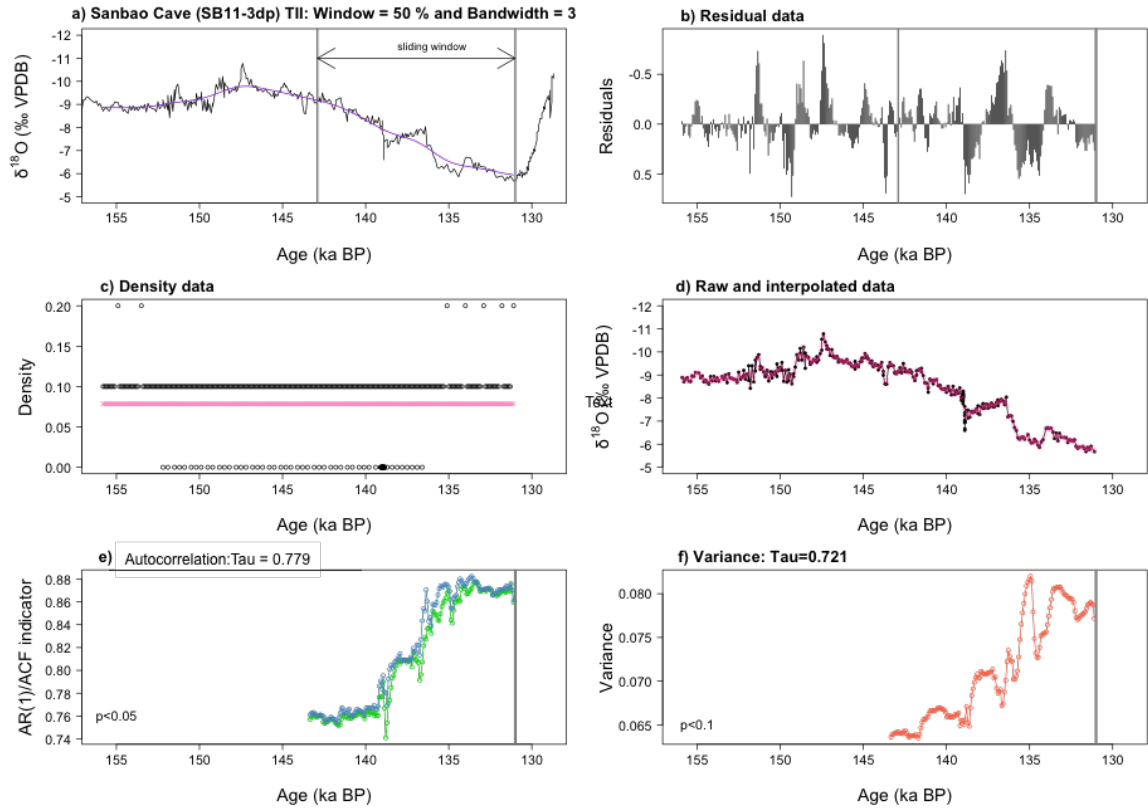
723 (Figure 4)

724



725

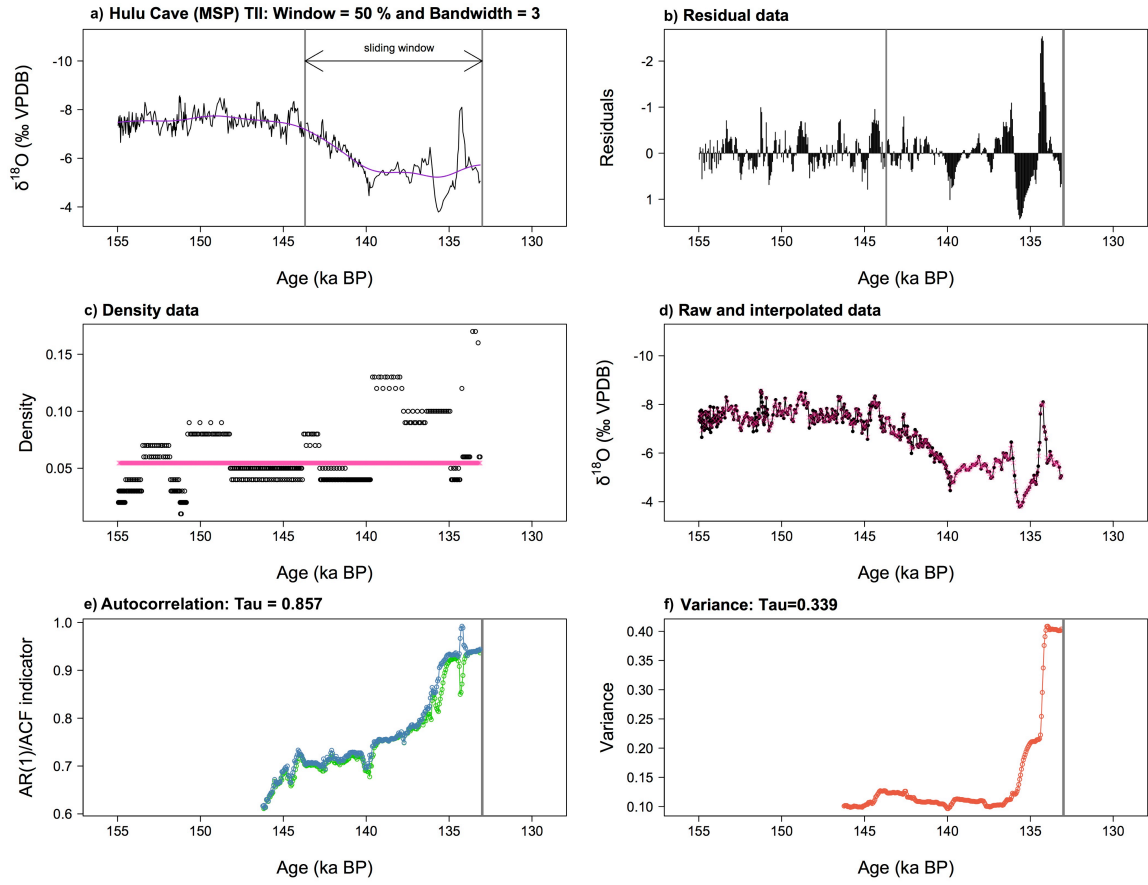
726 (Figure 5)



727

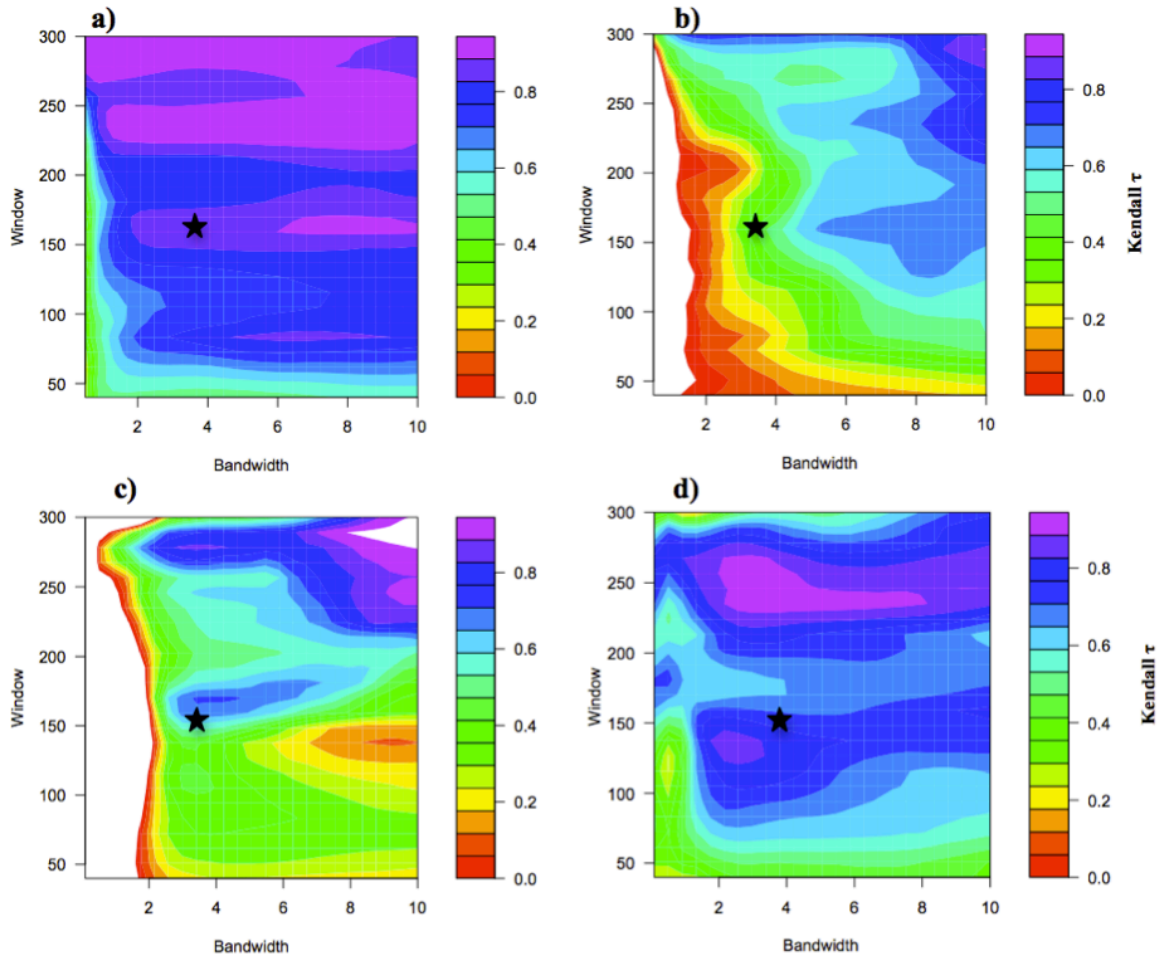
728 (Figure 6)

729



730

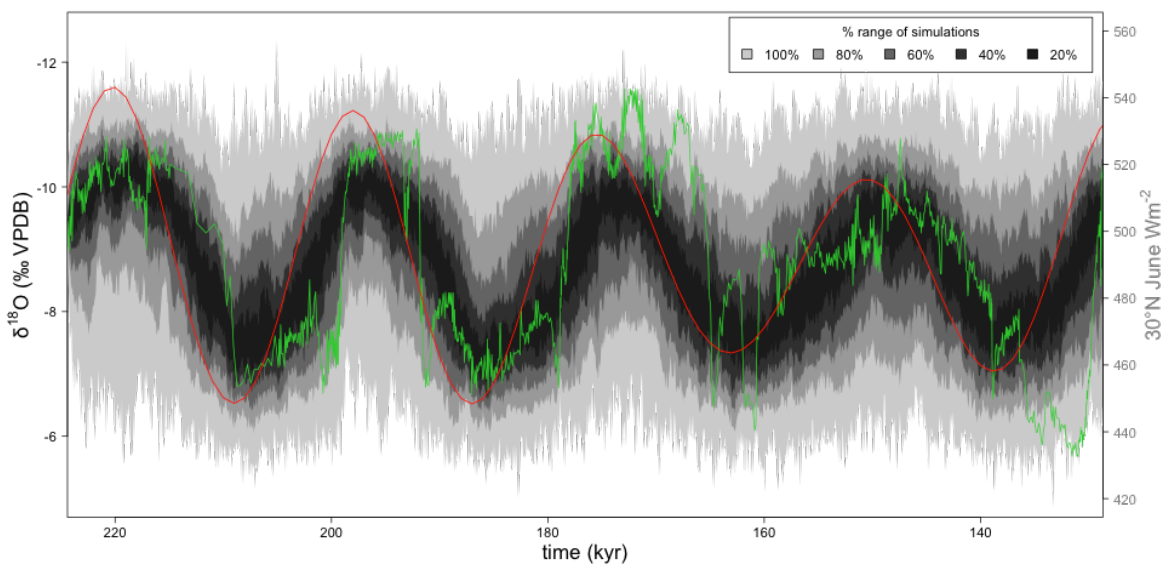
731 (Figure 7)



732

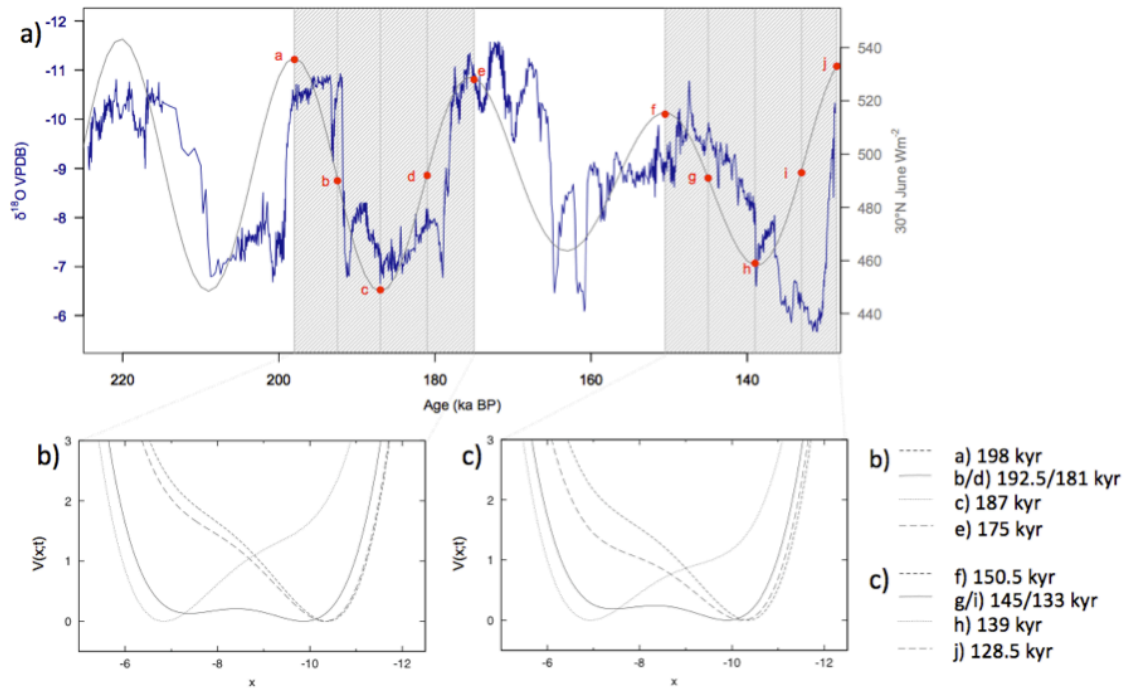
733 (Figure 8)

734



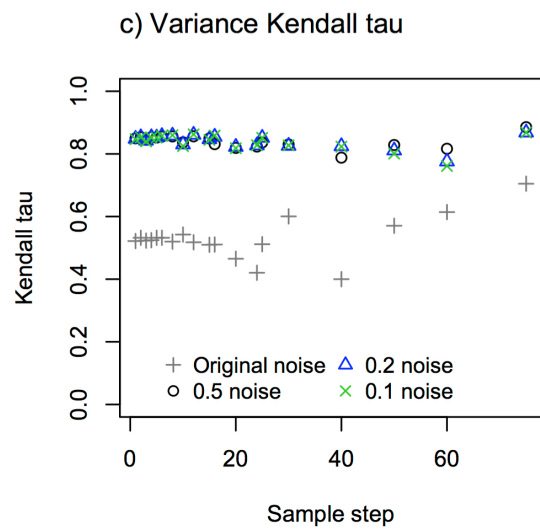
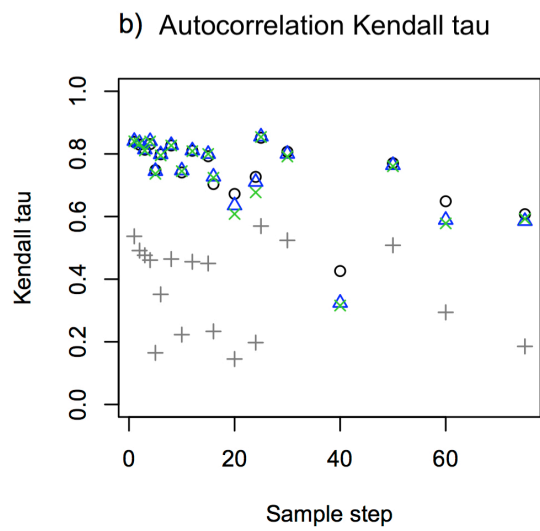
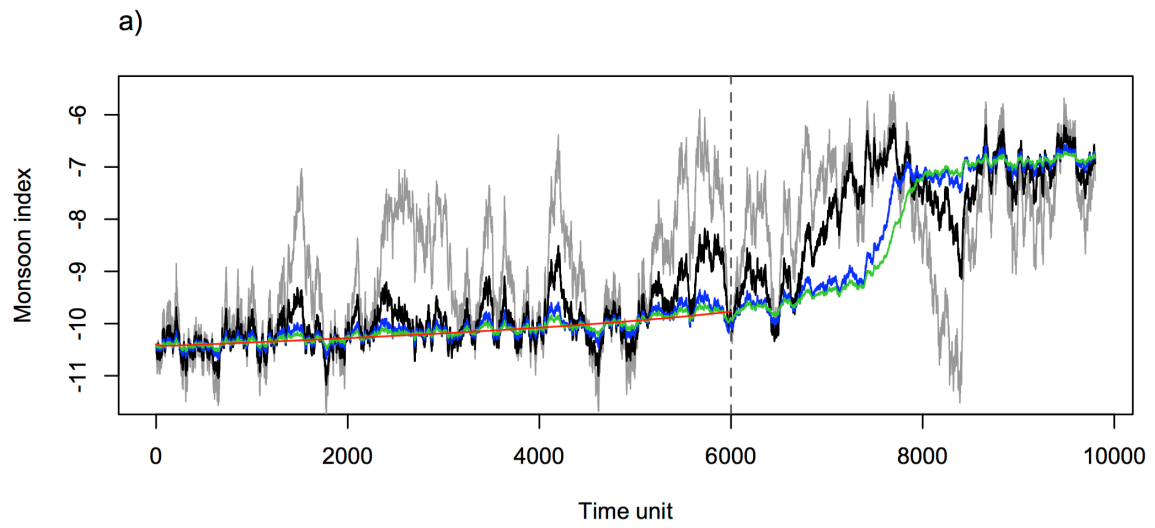
735

736 (Figure 9)



737

738 (Figure 10)



739

740 (Figure 11)